ACS Catalysis

pubs.acs.org/acscatalysis

Research Article

Elucidating Electron Transfer Kinetics and Optimizing System Performance for *Escherichia coli*-Based Semi-Artificial H_2 Production

Mira T. Gamache, Rima Charaf, Larissa Kurth, Dawit T. Filmon, Moritz Senger, Nicolas Plumeré, Leif Hammarström, and Gustav Berggren*

Cite This: *ACS Catal.* 2023, 13, 9476–9486

Read Online

ACCESS | Metrics & More | Article Recommendations | Supporting Information

ABSTRACT: Both photo- and biocatalysis are well-established and intensively studied. The combination of these two approaches is also an emerging research field, commonly referred to as semi-artificial photosynthesis. Semi-artificial photosynthesis aims at combining highly efficient synthetic light harvesters with the self-healing and potent catalytic properties of biocatalysis. In this study, a semi-artificial photocatalytic system featuring *Escherichia coli* bacteria, which heterologously express the [FeFe] hydrogenase enzyme HydA1 from green algae, is employed as a hydrogen gas production catalyst. To probe the influence of photochemistry on overall system performance, the *E. coli* whole-cell catalyst is combined with two different photosensitizers and redox mediators. The addition of a redox mediator greatly improves the rates and longevity of the photocatalytic system, as reflected in increases of both the turn-over number (0.777 vs 10.9 μmol H_2 mL^{-1} $OD_{600}{}^{-1}$) and the turn-over frequency (175 vs 334 μmol H_2 mL^{-1} h^{-1} $OD_{600}{}^{-1}$). The redox mediator is found to both protect from photobleaching and enable electron transport to the hydrogenase from an extracellular photosensitizer. However, *E. coli* cells are strongly affected by the photocatalytic system, leading to a decrease in cell integrity and cell viability, possibly due to toxic decomposition products formed during the photocatalytic process. We furthermore employed steady-state and transient absorption spectroscopy to investigate solution potentials and the kinetics of electron transfer processes between the sacrificial electron donor, photosensitizer, redox mediator, and the [FeFe] hydrogenase as the final electron acceptor. These results allowed us to rationalize the different activities observed in photocatalytic assays and offer a better understanding of the factors that influence the photocatalytic performance of *E. coli*-based whole-cell systems.

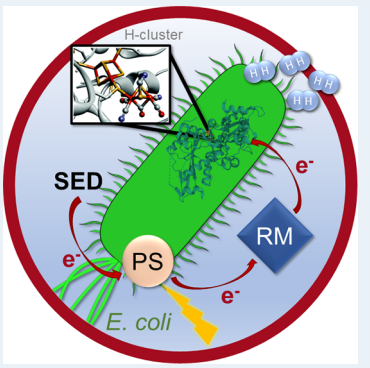

KEYWORDS: *hydrogenase, whole-cell catalysis, semi-artificial photosynthesis, hydrogen, transient absorption, redox mediator, sacrificial electron donor*

INTRODUCTION

Since the industrial revolution, fossil fuels have grown to become the main energy resource worldwide, resulting in increased emissions of greenhouse gasses such as carbon dioxide. The results of this stress on our environment can be felt globally. While many different approaches are needed to tackle the negative impacts of our society on the environment, a complete shift toward renewable energy resources is an important step.[1] To achieve this, a variety of strategies to harvest, transform, and store energy from different renewable sources are in use and under further development.

The most abundant energy resource we have on earth is radiation from the sun.[2] Current applications commonly transform solar energy into electricity or heat. However, another possibility is the photosynthesis of solar fuels. Natural photosynthesis provides a good example of processes making use of solar energy to synthesize a number of valuable products, all while functioning under mild conditions and without the use of rare metals.[3] In the context of solar fuels and a future hydrogen society, enzymes capable of oxidizing or producing molecular hydrogen have gained a lot of interest. Among these enzymes, the so-called [FeFe] hydrogenases are of particular interest due to their high turn-over frequencies (TOFs) and energy efficiencies.[4] While photosynthetic microorganisms expressing [FeFe] hydrogenases do benefit from the ability to regenerate the catalyst, they often struggle with low efficiencies of the natural photosystem.[5] Hence, various combinations of hydrogenases or molecular mimics with artificial photosystems have been widely studied.[6,7] Yet, these systems usually require costly enzyme purification, hindering industrial upscaling. This limitation has led to the more recent development of a variety of whole-cell-based biohybrid systems.[5,8−12]

Escherichia coli (*E. coli*) bacteria are often chosen as a host organism, and artificial photosensitizers (PSs) are added to

Received: March 24, 2023
Revised: June 14, 2023
Published: July 3, 2023

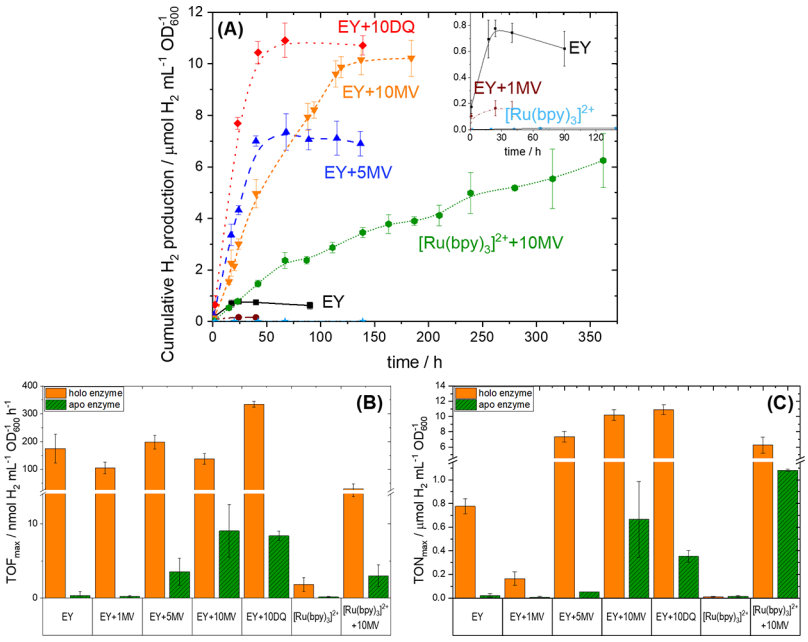

Figure 1. Photocatalytic hydrogen evolution assays exploring the effect of PSs and RMs on system performance. Samples contain a cell suspension in 100 mM PBS buffer at pH = 7.5, with 100 μM PS (EY or $[Ru(bpy)_3]^{2+}$), different concentrations of RM (MV or DQ, concentrations given in equivalents relative to PS), and 100 mM TEOA. Experiments are carried out under an inert gas atmosphere with continuous light irradiation. (A) Cumulative hydrogen production; inset: zoom-in for low-TON samples; (B) maximum TOF for samples both with holo-enzyme and apo-enzyme; and (C) maximum turn-over number (TON) reached for samples both with holo-enzyme and apo-enzyme. Note the broken Y axis in panels B and C.

Table 1. Summary of Photocatalytic Assay Results[a]

PS	eq RM[b]	[FeFe] hydrogenase[c]	Time/h	TOF_{max}/nmol H_2 mL^{-1} h^{-1} OD_{600}^{-1}	TON_{max}/μmol H_2 mL^{-1} OD_{600}^{-1}
EY		holo	24	175 ± 52	0.78 ± 0.06
EY		apo	24	0.4 ± 0.5	0.023 ± 0.017
EY	1 MV	holo	24	105 ± 21	0.17 ± 0.06
EY	1 MV	apo	24	0.2 ± 0.1	0.009 ± 0.005
EY	5 MV	holo	115	198 ± 24	7.4 ± 0.7
EY	5 MV	apo	89	3.5 ± 1.8	0.0532 ± 0.0002
EY	10 MV	holo	184	138 ± 19	10.2 ± 0.7
EY	10 MV	apo	88	9.0 ± 3.5	0.67 ± 0.32
EY[d]	10 MV	holo	100	271 ± 28	11.3 ± 0.4
EY	10 DQ	holo	67	334 ± 10	10.9 ± 0.7
EY	10 DQ	apo	67	8.3 ± 0.6	0.35 ± 0.05
EY[d]	10 DQ	holo	100	453 ± 47	10.6 ± 0.7
$[Ru(bpy)_3]^{2+}$		holo	67	1.8 ± 0.9	0.012 ± 0.004
$[Ru(bpy)_3]^{2+}$		apo	67	0.2 ± 0.1	0.015 ± 0.007
$[Ru(bpy)_3]^{2+}$	10 MV	holo	360	30 ± 17	6.2 ± 1.0
$[Ru(bpy)_3]^{2+}$	10 MV	apo	350	3.0 ± 1.5	1.081 ± 0.009

[a]Samples contain 100 μM PS, TEOA (100 mM), RM (0−1 mM, given in equivalents to PS), and cells (OD_{600} = 5) in 100 mM PBS (pH = 7.5). Experiments are conducted under an inert gas atmosphere. [b]Equivalents (eq) given relative to the PS concentration (100 μM). [c]Holo refers to cells containing the active holo-enzyme, generated through artificial maturation with $[Fe_2(adt)(CO)_4(CN)_2](Et_4N)_2$; apo refers to cells containing the inactive apo-enzyme as expressed by *E. coli*. [d]Samples containing higher TEOA concentrations (500 mM).

either improve the fermentative processes inside the cell host[13] or to deliver electrons to an overexpressed enzyme such as hydrogenases.[9,11,14] A variety of artificial PSs have been studied for whole-cell catalysis, e.g., inorganic materials such as TiO_2 nanoparticles,[15,16] metal oxynitrides,[9] CdS quantum dots,[11,17,18] or organic dyes such as Eosin Y (EY).[10,19] Furthermore, different (sacrificial) electron donors are added to the system. Typical examples of such electron donors found in the literature are cysteine,[8,17,20] triethanolamine (TEOA),[9,19] bis-trismethane,[11] and ascorbic acid.[13,21] While a system consisting of a whole-cell biocatalyst, an artificial PS, and an electron donor is technically a complete photocatalytic system, many reports also include a mediator, e.g., methyl viologen[9] or reduced graphene oxide,[21] which facilitates the efficient transport of electrons from the photoactive system to the enzyme. However, despite the continuously growing number of reported semi-artificial systems for photocatalytic hydrogen evolution, there is still a general shortage of mechanistic understanding of these highly complex whole-cell systems.[7,18]

https://doi.org/10.1021/acscatal.3c01347
ACS Catal. 2023, 13, 9476−9486

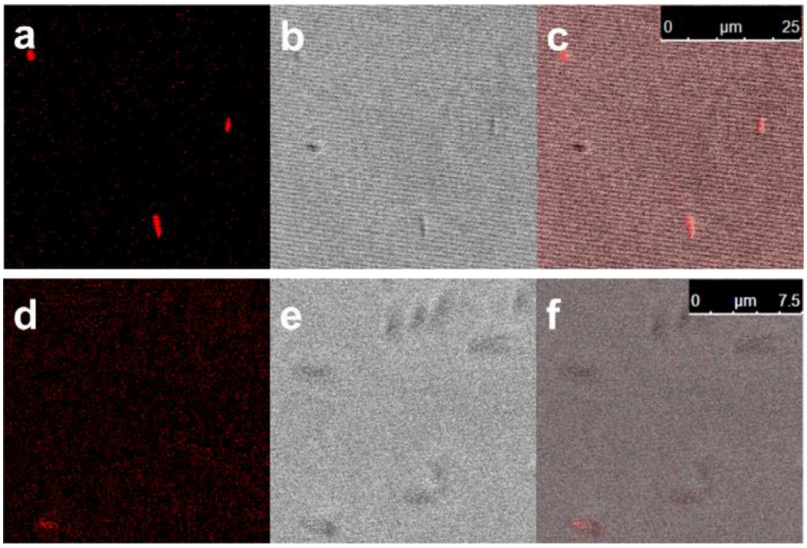

Figure 2. Confocal fluorescence microscopy images of cells after incubation with PS (EY or $[Ru(bpy)_3]^{2+}$) and subsequent separation from the supernatant through centrifugation. (Top) EY: excitation at 514 nm, emission at 550−600 nm; (a) emission image; (b) bright-field image; and (c) overlay of emission and bright-field images. Scale bar 25 μm. (Bottom) $[Ru(bpy)_3]^{2+}$: excitation at 458 nm, emission at 580−700 nm; (d) emission image; (e) bright-field image; and (f) overlay of emission and bright-field images. Scale bar 7.5 μm.

We and others have previously studied a semi-artificial system based on *E. coli* bacteria which heterologously express the [FeFe] hydrogenase, with EY as the artificial PS and TEOA as the sacrificial electron donor (SED) for light-driven hydrogen production.[10,12,19] We could further spectroscopically show that this hydrogen production activity indeed stems from the photocatalytically driven [FeFe] hydrogenase enzyme inside the cells.[19] Following our earlier design-of-experiment screening for the ideal catalytic conditions, we herein present studies focusing on the photochemistry aspects of the system. The factors determining the photocatalytic performance are identified using in vitro and in vivo steady-state and transient UV−vis absorption spectroscopy. We furthermore show that the choice of the redox mediator (RM) strongly influences not only the hydrogen evolution performance in terms of TOFs and final yields but also greatly affects the cell viability and present spectroscopic investigations of the mechanism involving the whole-cell system, which has to date been rarely discussed in the literature.

RESULTS AND DISCUSSION

Photocatalytic Assays. We used standard BL21(DE3) *E. coli* bacteria to heterologously express the apo-[FeFe] hydrogenase enzyme HydA1 from the green algae *Chlamydomonas reinhardtii* (*Cr*HydA1). Following protein expression and formation of the active holo-enzyme, the cells were suspended in phosphate-buffered saline (PBS) (pH = 7.5), yielding an optical density at 600 nm (OD_{600}) of 5. The enzyme was activated using artificial maturation to ensure a well-defined intracellular concentration of the active enzyme at a defined time point.[22,23] To form a photocatalytic system, TEOA was added as the SED, and EY or ruthenium tris-2-2′-bipyridine ($[Ru(bpy)_3]^{2+}$) was used as the PS. The protocol and concentrations of the different components were adapted from our previous design-of-experiment study on *E. coli*-based photocatalytic hydrogen evolution systems.[19] Control samples with *E. coli* cells containing an inactive apo-form of *Cr*HydA1 were analyzed in parallel. The samples (1 mL sample volume in 9 mL vials, estimated path length 5 mm) were prepared under an inert gas atmosphere (nitrogen or argon gas) and exposed to continuous white light irradiation (4000 lx, main emission 400−650 nm, spectrum, see Figure S.I. 5) at 30 °C. The headspace was sampled via gas chromatography at selected time points. The results of these photocatalytic assays are shown in Figure 1 and are summarized in Table 1.

As previously reported,[10,19] the whole-cell system using EY as the PS does produce hydrogen upon white light irradiation, and the photocatalytic system significantly outperforms the fermentative production in darkness.[22,23] However, the hydrogen production does not last longer than 24 h. One of the main reasons for the short-lived activity of the system is the decomposition of EY upon photoreduction by TEOA, apparent from a color change of the assay mix from pink to almost colorless. Similar decomposition of EY and structurally related dyes during photocatalysis has been previously reported by different groups and was suggested to involve dehalogenation.[24]

The metal-based PS $[Ru(bpy)_3]^{2+}$ is expected to be more stable under the catalytic conditions than EY. However, in the absence of an RM, no significant hydrogen evolution could be observed presumably due to the inability of $[Ru(bpy)_3]^{2+}$ to permeate the cell membrane.[25] Conversely, EY is a known cytoplasmic staining agent.[26] Indeed, confocal fluorescence microscopy (Figure 2) shows that EY is found inside the *E. coli* cytoplasm. This can be seen by the fact that the cells display clear fluorescence signals, which also appear evenly stained throughout, rather than exhibiting a stronger emission on the edge, which would be indicative of EY being located in the periplasm or on the outside of the cell. Meanwhile, barely any $[Ru(bpy)_3]^{2+}$ can be observed in or on the cells, hence showing the lack of membrane permeability of the Ru complex. The extracellular character of $[Ru(bpy)_3]^{2+}$ results in a lack of electron transfer into the cells and to the catalyst.

The instability of EY is primarily due to the degradation of the reductively quenched intermediate EY_{red}. Despite the intracellular localization of EY, the electron transfer from the reduced PS to the hydrogenase, or an alternative primary electron acceptor, is evidently insufficient to fully prevent

https://doi.org/10.1021/acscatal.3c01347
ACS Catal. 2023, 13, 9476−9486

degradation of the PS. An RM was hence introduced to act as a more efficient electron acceptor for EY as well as an electron shuttle for $[Ru(bpy)_3]^{2+}$. Methyl viologen (1,1′-dimethyl-4,4′-bipyridinium, MV) was selected as it is a well-established electron transfer agent to the hydrogenase enzyme, both in in vitro and in vivo systems.[12,16,27] Furthermore, a diquat derivative (1,1′-(1,3-propylene)-5,5′-dimethyl-2,2′-bipyridinium, DQ) was also assayed. DQ was selected due to its more negative reduction potential (−660 mV vs SHE[28]), relative to MV (−446 mV vs SHE[29]), providing a higher driving force for the electron transfer toward the hydrogenase (−400 mV vs SHE[30]). Earlier studies have shown that MV can slowly permeate the membrane of *E. coli*.[31] Furthermore, MV is capable of driving whole-cell hydrogen evolution.[12,32] To the best of our knowledge, there are no studies on the cell permeability of the herein-used DQ. However, we expect it to behave similarly to MV concerning membrane permeability.

To probe the effect of the RM concentration, different concentrations of MV were used in systems with EY as the PS. The results are shown in Figure 1 and Table 1. When one equivalent of MV with respect to EY is used, the observed hydrogen production is decreased (1 MV, 100 μM; Figure 1A, inset, brown trace). However, by increasing the MV concentration to 5 or 10 equivalents, both the initial rate (TOF) and the overall turn-over numbers (TONs) are increased (5 MV and 10 MV, i.e., 500 μM and 1000 μM, Figure 1A, blue and orange traces, respectively). The increase in TON correlated with the amount of MV added while the initial hydrogen production rate was highest with 5 rather than 10 equivalents of MV. The use of DQ as the RM results in the highest observed TOF (Figure 1A, red trace), equaling an apparent quantum yield of up to 4.8% (see Section S.I.1.7). However, the final TON is within error identical when comparing samples containing 10 equivalents of DQ or MV (Figure 1A, compare red and orange traces). When $[Ru(bpy)_3]^{2+}$ is used as the PS in the presence of 10 equivalents of MV (Figure 1A, green trace), a prolonged hydrogen evolution activity can be observed. However, the initial rate and the maximum TON reached in the studied time window are lower than those obtained with EY.

These observations provide several insights into the system. First, samples with EY and the apo-enzyme (lacking the H-cluster) exhibit very low hydrogen evolution activity (well below 10% compared to the holo-enzyme) and are hence practically catalytically inactive. $[Ru(bpy)_3]^{2+}$ in combination with MV results in a slightly higher background hydrogen production activity, and experiments with *E. coli* cells only containing the apo-[FeFe] hydrogenase exhibit almost 20% of the activity compared to the holo-enzyme. This activity in the absence of an active catalyst presumably stems from nanoparticle formation involving either $[Ru(bpy)_3]^{2+}$ or other trace metals in the cell, e.g., forming metal oxides or metallic particles, which are then catalytically active, a common phenomenon when dealing with molecular catalysts.[33] Alternatively, MV_{red} has also been reported as capable of yielding low levels of hydrogen production.[34] Yet, there is a strong increase in activity in the presence of the co-factor, hence leading to the conclusion that also in this system, the main hydrogen evolution activity stems from the hydrogenase enzyme.

Second, the implementation of an RM dramatically increases system performance. The RM acts as an efficient electron acceptor from both the reduced EY, EY_{red}, and the excited Ru complex, ($[Ru(bpy)_3]^{2+*}$). The formation of RM_{red} can be observed in both increased hydrogen evolution activity and color changes of the photocatalytic assay samples. In the case of MV, which exhibits a dark blue color in its reduced form, accumulation of MV_{red} could be observed upon light irradiation. This accumulation indicates that the electron transfer from MV_{red} to the hydrogenase is rate-limiting in this system.

Third, comparing systems containing MV and DQ, the diquat results in significantly higher rates. This is in line with the more negative reduction potential of DQ compared to MV and hence an expected increase in the electron transfer rate toward the hydrogenase.

Although a distinct difference in the TOF was observed, the choice of the RM did not affect the final hydrogen production. Both systems using EY and 10 equivalents of either MV or DQ yield a total of approximately 50−55 μmol of dihydrogen. With a total of 100 μmol of the SED being present in the system and two electrons necessary to produce one hydrogen molecule, it can be argued that the overall TON is limited by electron supply by the SED. However, we note that oxidized TEOA is known to form a strongly reducing radical and could consequently serve as a two-electron donor,[35] hence rendering higher TONs possible. Still, the fact that both systems (10 MV and 10 DQ) yield the same overall TON (see Figure 1A,C) implies that the supply of TEOA is a limiting factor in this system. Yet, the use of higher TEOA concentrations (500 mM instead of 100 mM) did not lead to a higher TON, regardless of the RM (see Figure S.I. 7). Similarly, the addition of TEOA at later points during the experiment (shortly before or after the maximum TON was reached) did not yield any significant differences.

However, an increase in initial TEOA concentrations did result in a corresponding increase in the initial TOF (271 nmol H_2 mL^{-1} h^{-1} $OD_{600}{}^{-1}$). This shows that the reductive quenching of EY by the SED is limiting the electron transfer from EY_{red} to MV and thus MV_{red} accumulation. By extension, this highlights the fact that a higher concentration of MV_{red} increases the electron transfer rate to the hydrogenase, implying that photochemistry controls overall rates.

Finally, the longevity of hydrogen evolution with $[Ru(bpy)_3]^{2+}$ is in line with the high stability of the PS. On the other hand, in systems with EY, it is assumed that while the RM does protect and greatly reduce photobleaching of the PS, eventual decomposition of the PS does play a role in the loss of activity. However, as observed with the SED, the addition of EY to the reaction mixtures shortly before or after the maximum TON was reached did not again result in a reactivation of the photocatalytic activity. We could furthermore exclude changes in pH being responsible for the loss of activity. Measurements before photocatalytic assays and after a maximum TON was reached revealed no significant deviation (±0.2) from the desired pH of 7.5. There have been reports of hydrogenation of MV during photocatalysis in the presence of a Pt catalyst[36] or under strongly acidic conditions.[37] Other studies observed photochemical or thermal decomposition products from MV in systems where no catalyst was present.[34,38] While we cannot rule out that these processes occur, we expect that under the herein chosen photocatalytic conditions, the degradation of MV is not the primary limiting factor.

Analogous photocatalytic experiments were furthermore carried out using cell lysates, i.e., after artificial maturation,

https://doi.org/10.1021/acscatal.3c01347
ACS Catal. 2023, 13, 9476−9486

the cells were lysed, and the suspension was then used to prepare photocatalytic samples. In all cases employing an RM, the observed initial TOF was larger than when non-lysed cells were used. This observation is well in line with previous studies indicating that cell lysis makes electron transfer from an RM to the enzyme more efficient.[31] However, the system appeared less stable, i.e., the maximum TONs reached are lower than when whole cells were used, showcasing the protective nature of the whole-cell scaffold (see Table S.I. 1 and Figure S.I. 8).

Overall, when comparing the observed TOFs with the values reported for the purified *Cr*HydA1 enzyme in the literature (specific activity of 600−700 μmol H_2 min^{-1} mg^{-1}),[39] we note that our observed TOFs are lower by 1−2 orders of magnitude. More specifically, based on previous studies,[23] we estimate 13.5 μg of the enzyme in each sample, which would equal a possible TOF of 8.1−9.5 μmol H_2 min^{-1}. Yet, the highest TOF observed herein is 37.8 nmol H_2 min^{-1}. This difference is not unexpected due to three main reasons. The reduced RM has to be transferred into the cells, which affects the overall rate of hydrogen evolution. Furthermore, the hydrogenase enzyme might not be the primary electron acceptor, resulting in additional electron transfer steps. In addition, the reaction conditions used to determine the TOF of [FeFe] hydrogenases commonly rely on much larger quantities of MV_{red} generated through chemical reduction. Thus, circumventing photogeneration of the electron donor, as also seen in this study, can affect the overall rate.

Cell Integrity and Viability Assays. The whole-cell scaffold introduces a variety of factors that can influence the catalytic performance. In return, the introduction of a photoactive system affects living organisms. We conducted cell integrity and viability assays of photocatalytic samples at different time points to elucidate the effect of the different photocatalytic components on *E. coli* cells.

In vitro assays were conducted to investigate the cell integrity in the photocatalytic experiments by determining whether the main hydrogen evolution activity stems from the enzyme present in the supernatant or inside the cells (Figures 3 and S.I. 9). The cells were separated from the supernatant via centrifugation, and following cell lysis, the hydrogenase activity of the two fractions was determined through MV−sodium dithionite assays.[22,23] It should be noted that the activity of the whole-cell fraction is generally underestimated, as it relies on complete lysis and release of the enzyme into the solution without loss of activity. While the nature of the assay prevents a quantitative comparison of the results, we can nonetheless draw some qualitative conclusions. First, when no RM is used, the main hydrogen evolution activity stems from the cells, in line with our previous study.[19] Second, in all systems using an RM, substantial amounts of the enzyme are present in the supernatant even before or after only short irradiation periods (Figure 3, left and Figure S.I. 9). Finally, a decrease of overall activity for longer times can be observed for systems using EY as the PS, highlighting that not only the photoactive component(s) of the catalytic system loses activity.

The decrease in cell integrity does not necessarily impair the overall performance of the photocatalytic system. Indeed, it has been reported that cell breakage increases the reactivity of MV with enzymes in *E. coli*, arguably due to increased access to the enzyme.[31] However, a key motivation for semi-artificial photosynthesis is the possibility of self-regeneration of the whole-cell catalyst, and it is critical to understand where the toxicity stems from to move toward more long-lived systems.

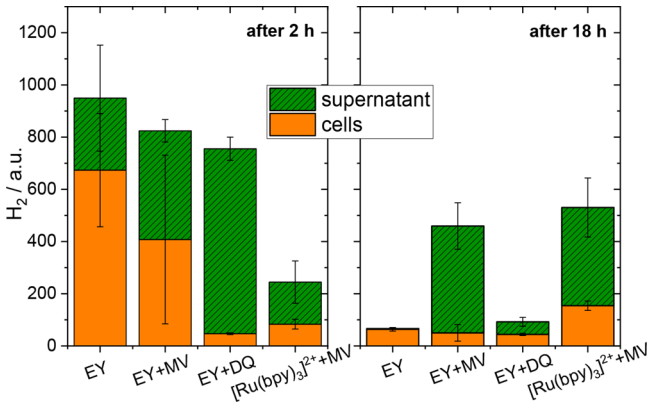

Figure 3. Comparison of hydrogen evolution activity stemming from the supernatant vs cells probed at different time points during photocatalysis. Activity was determined through NaDT/MV assays performed in 100 mM phosphate buffer at pH 6.8. Samples were taken after 2 (left) and 18 (right) h under photocatalytic conditions. All samples contained *E. coli* cells (OD_{600} = 5), combined with 100 μM EY ("**EY**"); 100 μM EY and 1 mM MV ("**EY + MV**"); 100 μM EY and 1 mM DQ ("**EY + DQ**"); or 100 μM $[Ru(bpy)_3]^{2+}$ and 1 mM MV ("$[$**Ru(bpy)**$_3]^{2+}$**+ **MV**").

We thus conducted viability studies, i.e., probed the ability of cells to replicate, in which samples from the different photocatalytic conditions were incubated in the dark or under light irradiation. Samples were collected after 18 and 40 h and plated on agar. The results are summarized in Table 2 and Figure S.I. 10.

Overall, the single components do not show any toxicity for the cells impairing their ability to replicate, with or without exposure to light irradiation. The one exception is MV, which was found to somewhat decrease the viability on a timescale of >18 h. Similarly, the combination of MV and TEOA also resulted in a larger decrease in viability than DQ and TEOA, although in both cases, a fraction of the cells remained viable even after 40 h of incubation. The presence of MV was also found to decrease the viability of cells under photoactive conditions. Cells in a suspension with the apo-enzyme including EY and TEOA were found to be viable following irradiation for 18 h in the absence and presence of DQ, but the addition of MV completely abolished viability. However, for the functional photocatalytic system, i.e., cell suspensions including the holo-enzyme, SED, and either EY (with or without RM) or $[Ru(bpy)_3]^{2+}$ (with RM), no cell viability was observed after light irradiation for 18 h.

The negative effects of MV on viability were somewhat unexpected. While it is well known that MV is toxic to cells under aerobic conditions due to the formation of reactive oxygen species (ROS), MV is reported to be non-toxic toward cells under anaerobic conditions.[40,41] The samples studied herein were prepared under strictly anaerobic conditions, and hence, the observed toxicity with MV is unlikely to stem from ROS formation. Furthermore, both MV and diquat derivatives have been reported to only weakly bind to DNA externally,[42] and it is hence unlikely that the cytotoxicity stems from DNA intercalation of the planar MV molecule. However, upon reduction, MV_{red} can also act as a reductant for other components present in the cell. Thus, broad interference with intracellular redox processes could contribute to toxicity.[41,43] Furthermore, it has been suggested that MV can cause NADPH depletion and act as a cytotoxin in the absence

https://doi.org/10.1021/acscatal.3c01347
ACS Catal. 2023, 13, 9476−9486

Table 2. Plating Studies of Different Samples Containing *E. coli* Cells (OD_{600} = 5), with Apo- or Holo-[FeFe] Hydrogenase, Suspended in 100 mM PBS Buffer (pH = 7.5) with Different Other Components Added[a]

	after 18 h				after 40 h			
	light		dark		light		dark	
	apo	holo	apo	holo	apo	holo	apo	holo
cells[b]	++++	++++	++++	++++	++++	++++	++++	++++
+EY[c]	++++	++++	++++	++++	++++	++++	++++	++++
+$[Ru(bpy)_3]^{2+}$[c]	++++	++++	++++	++++	++++	++++	++++	++++
+TEOA[d]	++++	++++	++++	++++	++++	++++	++++	++++
+MV[e]	++++	++++	++++	++++	+	+	++	+
+DQ[e]	++++	++++	++++	++++	++++	++++	++++	++++
+MV + TEOA	+++	+++	++++	++++	++	+	++++	+
+DQ + TEOA	++++	++++	++++	++++	+++	+++	++++	++++
+EY + TEOA	+++	−	++++	++++	+++	−	++++	++++
+$[Ru(bpy)_3]^{2+}$+TEOA	++++	++++	++++	++++	+++	+++	+++	+++
+EY + TEOA + MV	−	−	++	+	−	−	−	−
+EY + TEOA + DQ	++	−	++++	++++	−	−	++++	++++
+$[Ru(bpy)_3]^{2+}$+TEOA + MV	+	+	++++	++++	−	−	++++	++++

[a]Samples were plated after being kept under constant light irradiation (light) or in the dark (dark) at 30 °C for 18 or 40 h. Component combinations resulting in a significant drop in viability are highlighted in bold. For an explanation of ratings, see Figure S.I. 10. [b]All samples contained *E. coli* cells at an initial OD_{600} of 5. [c]+EY or +$[Ru(bpy)_3]^{2+}$ contains 100 μM of the respective PS. [d]+TEOA contains 100 mM of the SED. [e]+MV or +DQ contains 1 mM of the respective RM.

of oxygen. The latter effect could explain the observed MV toxicity in the absence of an active photosystem, which would be needed if MV_{red} was the toxic component.[41,43] Overall, the observation that viability improved when MV was replaced by DQ shows that these issues can be alleviated while still retaining the positive effect of the RM on catalytic performance.

Regardless of the RM, we note that all photocatalytically active systems assayed here displayed dramatic decreases in cell viability. Indeed, even the system with TEOA and EY shows no cell viability after light irradiation, despite the cell integrity assays indicating an active hydrogenase mainly inside intact cells. Thus, apparent cell integrity does not strictly correlate with cell viability. Overall, the decreased cell viability upon hydrogen evolution indicates that a toxic byproduct is formed under photocatalytic conditions. We postulate that decomposition products of oxidized TEOA are toxic to the cells and, among other things, induce a decrease in cell integrity. This explanation would account for the faster decrease of cell integrity with DQ than with MV under catalytic conditions (Figure 3), as the hydrogen evolution rate is much higher and hence more TEOA is oxidized. It is also in line with the much slower decrease of cell integrity when $[Ru(bpy)_3]^{2+}$ is used compared to EY as the PS. Furthermore, it could explain why cells with apo-hydrogenase are generally less affected as they do not offer an obvious terminal electron acceptor, and hence, less TEOA can be oxidized.

In Vitro and In Vivo Steady-State and Transient UV–Vis Absorption Spectroscopy. Based on the photocatalytic assay results, we could already draw some conclusions regarding the limiting electron transfer steps in our whole-cell system. Time-resolved absorption spectroscopy gives further insights into the electron transfer kinetics (all reported values are averages of three individual traces or more). A detailed discussion of the electron transfer processes occurring upon irradiation of the photoactive system with EY can be found in the SI (Section S.I. 6). In short, upon irradiation in the visible absorption band, EY is excited and undergoes intersystem crossing to a long-lived triplet excited state ^{3}EY*. This excited state is reductively quenched by TEOA. In the absence of a suitable electron acceptor, the reduced state, EY_{red}, is very long-lived [observed rate constant for decay is $(2.4 \pm 0.2) \times 10^{-2}$ s^{-1}, see Figures S.I. 15 and 4C, black trace] but eventually results in decomposition via hydrolysis or dehalogenation. At shorter timescales (<200 μs), only a slight decrease of the EY_{red} signal via unknown decay processes can be observed (see Figure 4A). When the hydrogenase (20 μM) is added to samples containing EY and TEOA, a recovery of the ground state absorption and a decrease of the reduced EY can be observed at a pseudo-first-order rate constant of $(4.0 \pm 1) \times 10^3$ s^{-1} (Figure 4B). This corresponds to a second-order electron transfer rate constant from the reduced EY to *Cr*HydA1 of $(8 \pm 7) \times 10^7$ M^{-1} s^{-1}. At much longer timescales (Figure 4C, green trace), no absorption signal of EY_{red} could be generated, despite very low hydrogenase concentrations (550 nM) and long light irradiation (10 s, LED centered at 530 nm). This supports the observations at shorter timescales, showing that there is electron transfer from the reduced EY to the hydrogenase at a timescale faster than what can be resolved in this latter experimental setup. An overview of the observed pseudo-first-order rate constants is given in Scheme 1.

When *E. coli* cells are added to a sample containing EY and TEOA, the reduced state decays with a very similar rate constant of $(4.0 \pm 0.2) \times 10^3$ s^{-1} (Figure S.I. 21, right), indicating that the cells also act as an electron acceptor. This observed rate constant for the ground state bleach recovery and reduced state decay was not influenced by cell density. Furthermore, the same experiments were carried out using cells that had expressed the apo-hydrogenase enzyme but were not matured, hence lacking the functional holo-enzyme. The observed rate constants were identical (within the experimental error, data not shown) to those obtained with cell suspensions containing the holo-hydrogenase. We conclude that under the chosen experimental conditions, we cannot see definitive spectroscopic evidence for electron transfer toward the [FeFe] hydrogenase itself as the primary electron acceptor inside the cells. Based on previous EPR studies,[23] we estimate

https://doi.org/10.1021/acscatal.3c01347
ACS Catal. 2023, 13, 9476−9486

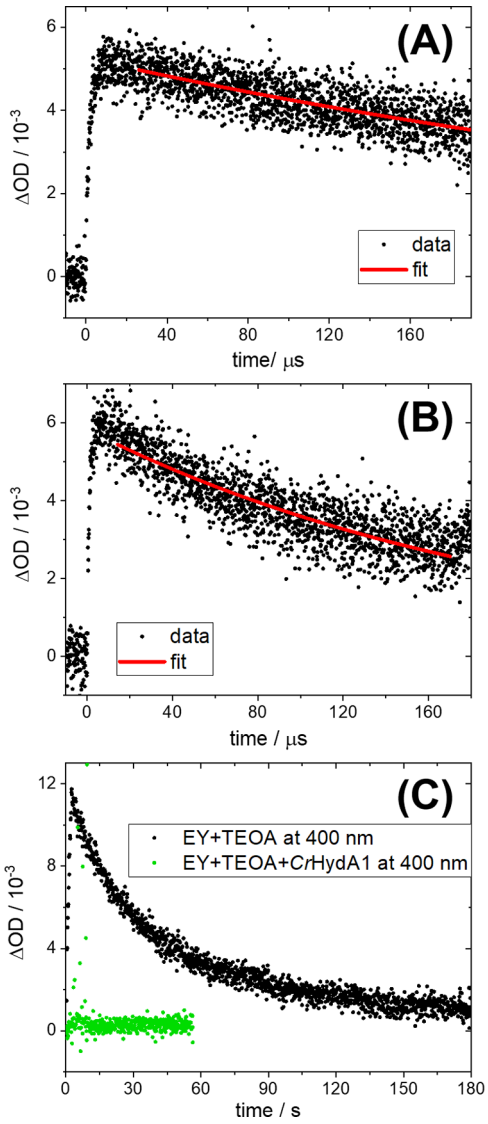

Figure 4. Kinetic traces of absorption changes at 400 nm upon excitation at 516 nm (A,B) or 530 nm (C). A: sample containing EY (4 μM) and TEOA (100 mM) in 100 mM PBS (1 cm path length). B: sample containing EY (13 μM), *Cr*HydA1 (20 μM), and TEOA (100 mM) in 100 mM PBS (1 mm path length). C: samples containing EY (4 μM) and TEOA (100 mM) in 100 mM PBS (3 s light irradiation, black trace) and in the presence of CrHydA1 (550 nM) (10 s light irradiation, green trace). Measurements were conducted under an inert gas atmosphere.

45,000 hydrogenase molecules per cell, resulting in an intracellular hydrogenase concentration of ≈70 μM. Thus, the intracellular concentration is on par with what was employed in the in vitro experiments. The absence of a distinct rate enhancement in the presence of the holo-[FeFe] hydrogenase under whole-cell conditions compared to the apo-enzyme is arguably due to the wide range of available electron acceptors in the latter case.

When the system including MV is investigated using transient absorption spectroscopy, a fast electron transfer [$(2.5 \pm 0.5) \times 10^9$ M^{-1} s^{-1}] from the reduced EY to MV is observed, both in the presence and absence of cells (see Figures S.I. 17, 18, and 22). Due to the observed instability of the cells in the presence of MV, these experiments were consistently performed with fresh preparations. Still, exact

Scheme 1. Schematic Representation of the Photocatalytic Cycle Involving EY as the PS (4 μM), TEOA as the SED (100 mM), and Either MV (Red, 38 μM) or the Hydrogenase *Cr*HydA1 (Light Blue, 20 μM) or Cells (Green, OD_{600} = 0.3) as the Electron Acceptor[a]

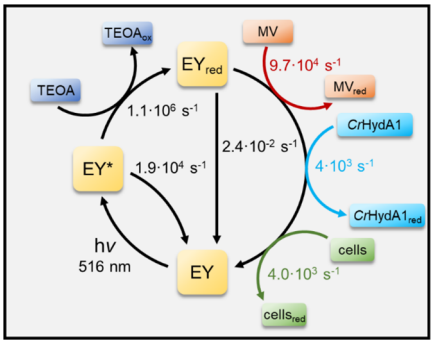

[a]Pseudo-first-order rate constants as obtained by transient absorption spectroscopy. Reported values are averages of three or more individual traces.

quantification of the MV_{red} to the cellular acceptor electron transfer step proved difficult as significant variations were observed over the course of the experiments (data not shown). Yet, it was evident that the reduced MV species is very long-lived, and in the presence of cells, the MV_{red} decay can be observed over the time course of several minutes. This indicates that the electron transfer from the reduced MV radical to an electron acceptor in the cell is much slower than that from the reduced EY to the cell. This is in line with relatively small electron transfer rates from MV_{red} to hydrogenase enzymes, which have been reported previously.[44] However, we note that in the whole-cell system, the electron transfer kinetics are also intertwined with mass-transfer kinetics related to the transport of RM_{red} to the target protein.

The apparent sluggishness of the electron transfer from the reduced MV can also be rationalized by the relatively low concentration of MV_{red} generated during the experiment. In return, this results in much larger concentrations of the oxidized MV, which can act as an electron acceptor from the reduced hydrogenase, resulting in significant back-electron transfer. To circumvent this issue, the transient spectroscopy analysis was complemented by steady-state UV−vis spectroscopy experiments to estimate how the thermodynamic driving force varies between the photocatalytic assays. As seen above, different initial rates of H_2 production are observed as a function of both the nature and the concentration of the RMs (Figure 1). This observation is assumed to be due to both the different reduction potentials and different ratios of the oxidized and reduced RM. On a molecular level, a high reduction potential of the mediator will ensure a strong driving force for forward electron transfer to the cellular electron acceptor and prohibit back-electron transfer. Similarly, a high RM_{red}/RM ratio is expected to increase the rate of forward electron transfer to the electron acceptor(s) and also limit the back-electron transfer. Redox potentials and concentrations of RM and RM_{red} can be summarized in the solution potential *E*, which is calculated using the Nernst equation (for details, see Section S.I. 6.4).

To estimate the solution potentials, we prepared solutions with TEOA and selected combinations of RMs and PSs. The solutions were subsequently irradiated with green (530 nm, for

https://doi.org/10.1021/acscatal.3c01347
ACS Catal. 2023, 13, 9476−9486

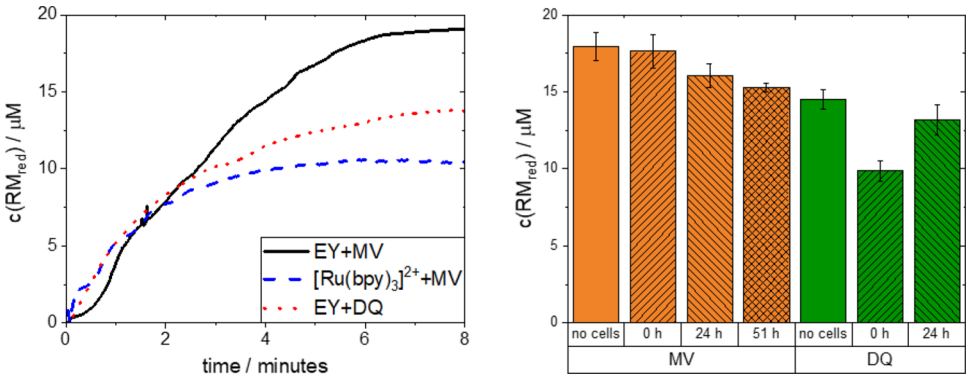

Figure 5. Accumulation of RM_{red} upon constant illumination in the absence and presence of *E. coli* cells. (Left) RM_{red} accumulation in the absence of cells, samples containing PS (4 μM), RM (20 μM), and TEOA (100 mM) in PBS (pH = 7.5). (Right) Comparison of (pseudo)-steady-state RM_{red} concentration in in vitro EY samples ("no cells") with in vivo samples taken from photocatalytic assays at different time points (0, 24, and 51 h); photocatalytic samples are diluted to yield an OD of 0.1, RM concentration of 20 μM; additional EY is added to yield a final concentration of 4 μM. All measurements are conducted under an inert gas atmosphere.

EY) or blue (447 nm, for $[Ru(bpy)_3]^{2+}$) light, and the accumulation of RM_{red} was monitored using UV−vis absorption spectroscopy. The concentration of RM_{red} was calculated using the reported extinction coefficients of MV_{red} (ε_{400nm} = 42,100 cm^{-1} M^{-1})[45] and DQ_{red} (ε_{400nm} = 11,500 cm^{-1} M^{-1}).[28] The concentrations of the PS and RM in the spectroscopic samples were lower than those in the photocatalytic assays due to their strong absorbance. Nevertheless, the relative differences between the assayed systems can still be assumed to hold true also under photocatalytic conditions. The results are shown in Figure 5 (left panel) with the calculated concentrations and solution potentials summarized in Table 3.

Table 3. Calculated Concentrations of Accumulated RM_{red} upon Continuous Illumination and Solution Potentials E^a

PS	RM	$c(RM_{red})/\mu M$	ratio RM_{red}/RM	solution potential E/mV vs SHE
EY	MV	17.9	8.5	−501 ± 13
$[Ru(bpy)_3]^{2+}$	MV	10.4	1.1	−448 ± 3
EY	DQ	14.5	2.6	−685 ± 4

[a]Sample solutions contain 4 μM PS, 20 μM RM, and 100 mM TEOA in the PBS solution (pH = 7.5); measurements are carried out under an inert gas atmosphere.

Comparing the two PSs, EY and $[Ru(bpy)_3]^{2+}$, at a constant MV concentration, EY yields a higher (pseudo)-steady-state concentration of MV_{red}. This is consistent with the different mechanisms expected for the electron transfer from the excited PS to MV. In contrast to EY, which follows a reductive quenching pathway (see Scheme 1), $[Ru(bpy)_3]^{2+}$ is expected to follow an oxidative quenching mechanism, i.e., the excited PS transfers an electron to an electron acceptor (e.g., MV). The oxidized complex then gets reduced again by the SED. Under continuous illumination, in both the reductive quenching process with EY and the oxidative quenching process with $[Ru(bpy)_3]^{2+}$, RM_{red} is accumulated. However, in the case of $[Ru(bpy)_3]^{2+}$, a lower concentration of accumulated RM_{red} is achieved (Figure 5). This is in line with the lower driving force for electron transfer from excited $[Ru(bpy)_3]^{2+*}$ to MV compared to electron transfer from EY_{red} to MV. Moreover, it is known that back-electron transfer from MV_{red} to photogenerated $[Ru(bpy)_3]^{3+}$ can occur, making oxidative quenching less efficient.[46] A similar back-electron transfer is unlikely to occur in the case of EY as EY_{red} returns to the ground state upon electron transfer, which makes back-electron transfer thermodynamically unfavorable. It follows that a lower MV_{red}/MV ratio is expected to contribute to the lower hydrogen production rates obtained with $[Ru(bpy)_3]^{2+}$ as compared to EY. Similar reasoning can also rationalize the dependence of initial rates on the MV concentration (compare 5 vs 10 equivalents of MV, Figure 1). As the rate constant for electron transfer from EY to MV is very large, both 5 and 10 mM give a near-unity yield of electron transfer. Instead, a lower initial MV concentration allows the MV_{red}/MV ratio to increase more quickly. In other words, the RM can be regarded as a redox buffer, and a lower initial MV concentration allows for a more rapid change of solution potential, which by extension changes the ratio of forward and back-electron transfer to and from the hydrogenase.

When the two RMs are compared, using EY as the PS, the maximum concentration of DQ_{red} is much lower than that of MV_{red}. This difference can be explained by the lower driving force for the reduction of DQ compared to MV by the reduced PS. Yet, the more negative reduction potential of DQ leads to a larger driving force for the subsequent electron transfer toward the cellular electron acceptor and decreases non-productive back-electron transfer, hence yielding a higher hydrogen production rate. This is in good agreement with the significantly more negative solution potential value for the DQ system than the MV system (−685 vs −504 mV), despite the lower DQ_{red} concentration.

Adding a catalyst to the system is expected to reduce the (pseudo)-steady-state RM_{red}/RM ratio through the consumption of RM_{red}. To examine how these ratios varied between assay conditions and with time, we compared samples with the different RMs at selected time points of the photocatalytic experiments. Samples were collected either before (0 h) or after operating the photocatalysis (for 24 or 51 h). The steady-state population of RM_{red} was again probed by UV−vis spectroscopy following exposure to continuous illumination and compared to analogous samples in which no *E. coli* cells were added (Figure 5, right, "no cells"). The results are shown in Figure 5 (right panel). When MV is used as the RM, the presence of fresh cells does not impact the accumulation of MV_{red} (Figure 5, right, MV 0 h time point), indicating that the

https://doi.org/10.1021/acscatal.3c01347
ACS Catal. 2023, 13, 9476−9486

electron transfer to the hydrogenase is slow and does not significantly affect the MV_{red} concentration. Samples taken at later time points, however, do show a slight decrease in the amount of accumulated MV_{red}, indicating that a more efficient or accessible electron acceptor becomes available during photocatalysis (Figure 5, right, MV 24 and 51 h time points). These results correspond well with the cell integrity assays discussed above (Figure 3). As the cell integrity decreases during catalysis, the hydrogenase enzyme and other cellular electron acceptors become more accessible for the RM over time.

When DQ is used, the presence of fresh cells strongly impacts the accumulation of DQ_{red} (Figure 5, right, DQ 0 h time point). As noted above, DQ_{red} has a larger driving force for electron transfer toward the hydrogenase than MV_{red}. This increased driving force will accelerate the electron transfer from DQ_{red}, causing a decrease in the steady-state DQ_{red} concentration. In contrast, cells that had been operating for 24 h under photocatalytic conditions had a much more limited effect on DQ_{red} accumulation (Figure 5, right, DQ 24 h time point). This latter observation agrees with a decay of the catalytic system on a daytime scale, as also noted in the photocatalytic assays (Figure 1A).

CONCLUSIONS

The work described herein presents a detailed characterization of an *E. coli*-based system for semi-artificial photosynthesis, ranging from factors controlling overall system performance and cell viability to a detailed elucidation of the photo-triggered electron transfer processes. The studied model system utilized a non-native [FeFe] hydrogenase for photocatalytic hydrogen evolution, and we expect the observed trends to hold true also for other *E. coli*-based systems depending on heterologously expressed (redox) enzymes. The implementation of an RM significantly improved overall performance and enabled the use of a wider range of PSs. We furthermore showed the impact that the concentration and reduction potentials of the RM have on the photocatalytic hydrogen evolution performance. It was found that the solution potential provided a highly useful tool for rationalizing the observed hydrogen production rates in different photocatalytic assays.

On a mechanistic level, transient spectroscopy showed that the electron transfer reaction from the PS to the target enzyme is most likely indirect, i.e., it proceeds via other redox-active components in the cell. This implies that further optimization of the system can be achieved by overexpressing suitable ferredoxins or, alternatively, by designing RMs with a higher affinity for the hydrogenase or other target enzymes.

We also note that the choice of the RM had a significant impact on cell viability, with the commonly employed MV displaying higher apparent toxicity than DQ. Nevertheless, we showed that the whole-cell system is strongly affected during photocatalysis, leading to both a decrease in cell integrity and cell viability. We propose that decomposition of the photocatalytic components or side products formed during photocatalytic hydrogen evolution exhibit significant toxicity to the host cell. Clearly, the identification of more biocompatible electron donors represents an important next step.

In closing, the presented *E. coli*-based semi-artificial system clearly offers the potential for long-lived photocatalytic hydrogen evolution without requiring time-intensive and elaborate enzyme purification. Yet, this study also highlights that to achieve a truly sustainable and self-healing photocatalytic system, it is necessary to reduce toxicity and stress on the cells. Exploring different SEDs and streamlining the electron transfer processes to overcome intracellular diffusion limitations appear to be critical for further improvement of these systems.

ASSOCIATED CONTENT

Supporting Information

The Supporting Information is available free of charge at https://pubs.acs.org/doi/10.1021/acscatal.3c01347.

Experimental details as well as additional data related to H_2 production assays, cell viability, and transient spectroscopy (PDF)

AUTHOR INFORMATION

Corresponding Author

Gustav Berggren − *Department of Chemistry—Ångström, Molecular Biomimetics, Uppsala University, 75120 Uppsala, Sweden;* orcid.org/0000-0002-6717-6612; Email: Gustav.berggren@kemi.uu.se

Authors

Mira T. Gamache − *Department of Chemistry—Ångström, Molecular Biomimetics, Uppsala University, 75120 Uppsala, Sweden;* orcid.org/0000-0002-6647-0916

Rima Charaf − *Department of Chemistry—Ångström, Physical Chemistry, Uppsala University, 75120 Uppsala, Sweden*

Larissa Kurth − *Department of Chemistry—Ångström, Molecular Biomimetics, Uppsala University, 75120 Uppsala, Sweden*

Dawit T. Filmon − *TUM Campus Straubing for Biotechnology and Sustainability, Technical University of Munich, 94315 Straubing, Germany*

Moritz Senger − *Department of Chemistry—Ångström, Molecular Biomimetics, Uppsala University, 75120 Uppsala, Sweden;* orcid.org/0000-0001-9225-4910

Nicolas Plumeré − *TUM Campus Straubing for Biotechnology and Sustainability, Technical University of Munich, 94315 Straubing, Germany;* orcid.org/0000-0002-5303-7865

Leif Hammarström − *Department of Chemistry—Ångström, Physical Chemistry, Uppsala University, 75120 Uppsala, Sweden;* orcid.org/0000-0002-9933-9084

Complete contact information is available at: https://pubs.acs.org/10.1021/acscatal.3c01347

Author Contributions

G.B. and M.G. conceived the project. M.G. carried out photocatalytic assays as well as studies on cell viability and integrity assays and handled data analysis under the guidance of G.B. and was supported by L.K. R.C. carried out all transient absorption spectroscopic experiments. M.S. performed proof-of-concept transient absorption spectroscopic experiments. L.H. advised on the transient spectroscopy studies and interpretation of the results. D.F. carried out the synthesis and analysis of the diquat derivative under the supervision of N.P. M.G. supplied the first manuscript draft, and all authors were involved in the analysis and revision of the manuscript. All authors have given approval to the final version of the manuscript.

https://doi.org/10.1021/acscatal.3c01347
ACS Catal. 2023, 13, 9476−9486

Funding

The Swedish Research Council (VR, grant no. 2021-04471 to G.B.), the Carl Trygger Foundation (grant no. 20:39 to G.B. and M.G.), the ANR-DFG "solar driven chemistry" (grant no. PL 746/5-1 to N. P.), and the Olle Engkvists stiftelse (grant no. 220-0226 to G.B. and M.S.) are gratefully acknowledged for funding.

Notes

The authors declare no competing financial interest.

■ ABBREVIATIONS

PS, photosensitizer; TEOA, triethanolamine; SED, sacrificial electron donor; TOF, turn-over frequency; TON, turn-over number; EY, Eosin Y; EY_{red}, one-electron reduced form of Eosin Y; MV, methyl viologen (1,1′-dimethyl-4,4′-bipyridinium); MV_{red}, one-electron reduced form of methyl viologen; RM, redox mediator; DQ, diquat derivative (1,1′-(1,3-propylene)-5,5′-dimethyl-2,2′-bipyridinium); $[Ru(bpy)_3]^{2+}$, ruthenium tris-2-2′-bipyridine

■ REFERENCES

(1) IEA; *Global Energy & CO2 status report. Technical Report*; International Energy Agency 2019.
(2) Philibert, C. *Solar energy perspectives*; OECD, 2011.
(3) Madavi, T. B.; Chauhan, S.; Keshri, A.; Alavilli, H.; Choi, K.-Y.; Pamidimarri, S. D. V. N. Whole-cell biocatalysis: Advancements toward the biosynthesis of fuels. *Biofuels, Bioprod. Biorefin.* **2022**, *16*, 859−876.
(4) (a) Lubitz, W.; Ogata, H.; Rüdiger, O.; Reijerse, E. Hydrogenases. *Chem. Rev.* **2014**, *114*, 4081−4148. (b) Lorenzi, M.; Berggren, G. [FeFe] Hydrogenases and Their Functional Models. In *Comprehensive Coordination Chemistry III*; Constable, E. C.; Parkin, G.; Que, Jr., L., Eds.; Elsevier, 2021; pp 731−756.
(5) Chen, J.; Li, Q.; Wang, L.; Fan, C.; Liu, H. Advances in Whole-Cell Photobiological Hydrogen Production. *Adv. NanoBiomed Res.* **2021**, *1*, No. 2000051.
(6) (a) Adam, D.; Bösche, L.; Castañeda-Losada, L.; Winkler, M.; Apfel, U.-P.; Happe, T. Sunlight-Dependent Hydrogen Production by Photosensitizer/Hydrogenase Systems. *ChemSusChem* **2017**, *10*, 894−902. (b) Okura, I.; Kim-Thuan, N. Kinetic studies of photoinduced methyl viologen reduction with ruthenium complexes and hydrogen evolution from water by hydrogenase. *J. Chem. Soc., Faraday Trans. 1* **1981**, *77*, 1411−1415. (c) Marguet, S. C.; Stevenson, M. J.; Shafaat, H. S. Intramolecular Electron Transfer Governs Photoinduced Hydrogen Evolution by Nickel-Substituted Rubredoxin: Resolving Elementary Steps in Solar Fuel Generation. *J. Phys. Chem. B* **2019**, *123*, 9792−9800. (d) Schmermund, L.; Jurkaš, V.; Özgen, F. F.; Barone, G. D.; Büchsenschütz, H. C.; Winkler, C. K.; Schmidt, S.; Kourist, R.; Kroutil, W. Photo-Biocatalysis: Biotransformations in the Presence of Light. *ACS Catal.* **2019**, *9*, 4115−4144. (e) Holá, K.; Pavliuk, M. V.; Németh, B.; Huang, P.; Zdražil, L.; Land, H.; Berggren, G.; Tian, H. Carbon Dots and [FeFe] Hydrogenase Biohybrid Assemblies for Efficient Light-Driven Hydrogen Evolution. *ACS Catal.* **2020**, *10*, 9943−9952. (f) Kornienko, N.; Zhang, J. Z.; Sakimoto, K. K.; Yang, P.; Reisner, E. Interfacing nature's catalytic machinery with synthetic materials for semi-artificial photosynthesis. *Nat. Nanotechnol.* **2018**, *13*, 890−899.
(7) Fang, X.; Kalathil, S.; Reisner, E. Semi-biological approaches to solar-to-chemical conversion. *Chem. Soc. Rev.* **2020**, *49*, 4926−4952.
(8) Shi, S.; Zeng, C.; Si, T.; Wang, B.; Wong, P. K. Photobiocatalytic Solar Fuel and Solar Chemical Conversion: Sufficient Activity and Better Selectivity. *ACS EST Engg.* **2022**, *2*, 989−1000.
(9) Kosem, N.; Honda, Y.; Watanabe, M.; Takagaki, A.; Tehrani, Z. P.; Haydous, F.; Lippert, T.; Ishihara, T. Photobiocatalytic H_2 evolution of GaN:ZnO and [FeFe]-hydrogenase recombinant Escherichia coli. *Catal. Sci. Technol.* **2020**, *10*, 4042−4052.
(10) Honda, Y.; Shinohara, Y.; Fujii, H. Visible light-driven, external mediator-free H2 production by a combination of a photosensitizer and a whole-cell biocatalyst: Escherichia coli expressing [FeFe]-hydrogenase and maturase genes. *Catal. Sci. Technol.* **2020**, *10*, 6006−6012.
(11) Honda, Y.; Shinohara, Y.; Watanabe, M.; Ishihara, T.; Fujii, H. Photo-biohydrogen Production by Photosensitization with Biologically Precipitated Cadmium Sulfide in Hydrogen-Forming Recombinant Escherichia coli. *ChemBioChem* **2020**, *21*, 3389−3397.
(12) Honda, Y.; Hagiwara, H.; Ida, S.; Ishihara, T. Application to Photocatalytic H2 Production of a Whole-Cell Reaction by Recombinant Escherichia coli Cells Expressing [FeFe]-Hydrogenase and Maturases Genes. *Angew. Chem., Int. Ed.* **2016**, *55*, 8045−8048.
(13) Ramprakash, B.; Incharoensakdi, A. Light-driven biological hydrogen production by Escherichia coli mediated by TiO_2 nanoparticles. *Int. J. Hydrogen Energy* **2020**, *45*, 6254−6261.
(14) Li, L.; Xu, Z.; Huang, X. Whole-Cell-Based Photosynthetic Biohybrid Systems for Energy and Environmental Applications. *ChemPlusChem* **2021**, *86*, 1021−1036.
(15) Ramprakash, B.; Incharoensakdi, A. Alginate encapsulated nanobio-hybrid system enables improvement of photocatalytic biohydrogen production in the presence of oxygen. *Int. J. Hydrogen Energy* **2022**, *47*, 11492−11499.
(16) Honda, Y.; Watanabe, M.; Hagiwara, H.; Ida, S.; Ishihara, T. Inorganic/whole-cell biohybrid photocatalyst for highly efficient hydrogen production from water. *Appl. Catal., B* **2017**, *210*, 400−406.
(17) Martins, M.; Toste, C.; Pereira, I. A. C. Enhanced Light-Driven Hydrogen Production by Self-Photosensitized Biohybrid Systems. *Angew. Chem., Int. Ed.* **2021**, *60*, 9055.
(18) Kornienko, N.; Sakimoto, K. K.; Herlihy, D. M.; Nguyen, S. C.; Alivisatos, A. P.; Harris, C. B.; Schwartzberg, A.; Yang, P. Spectroscopic elucidation of energy transfer in hybrid inorganic−biological organisms for solar-to-chemical production. *Proc. Natl. Acad. Sci. U. S. A.* **2016**, *113*, 11750−11755.
(19) Lorenzi, M.; Gamache, M. T.; Redman, H. J.; Land, H.; Senger, M.; Berggren, G. Light-Driven [FeFe] Hydrogenase Based H2 Production in E. coli: A Model Reaction for Exploring E. coli Based Semiartificial Photosynthetic Systems. *ACS Sustainable Chem. Eng.* **2022**, *10*, 10760−10767.
(20) Sakimoto, K. K.; Zhang, S. J.; Yang, P. Cysteine−Cystine Photoregeneration for Oxygenic Photosynthesis of Acetic Acid from CO_2 by a Tandem Inorganic−Biological Hybrid System. *Nano Lett.* **2016**, *16*, 5883−5887.
(21) Shen, H.; Wang, Y.-Z.; Liu, G.; Li, L.; Xia, R.; Luo, B.; Wang, J.; Suo, D.; Shi, W.; Yong, Y.-C. A Whole-Cell Inorganic-Biohybrid System Integrated by Reduced Graphene Oxide for Boosting Solar Hydrogen Production. *ACS Catal.* **2020**, *10*, 13290−13295.
(22) Khanna, N.; Esmieu, C.; Mészáros, L. S.; Lindblad, P.; Berggren, G. In vivo activation of an [FeFe] hydrogenase using synthetic cofactors. *Energy Environ. Sci.* **2017**, *10*, 1563−1567.
(23) Mészáros, L. S.; Ceccaldi, P.; Lorenzi, M.; Redman, H. J.; Pfitzner, E.; Heberle, J.; Senger, M.; Stripp, S. T.; Berggren, G. Spectroscopic investigations under whole-cell conditions provide new insight into the metal hydride chemistry of [FeFe]-hydrogenase. *Chem. Sci.* **2020**, *11*, 4608−4617.
(24) (a) Lazarides, T.; McCormick, T.; Du, P.; Luo, G.; Lindley, B.; Eisenberg, R. Making Hydrogen from Water Using a Homogeneous System Without Noble Metals. *J. Am. Chem. Soc.* **2009**, *131*, 9192−9194. (b) Alvarez-Martin, A.; Trashin, S.; Cuykx, M.; Covaci, A.; De Wael, K.; Janssens, K. Photodegradation mechanisms and kinetics of Eosin-Y in oxic and anoxic conditions. *Dyes Pigm.* **2017**, *145*, 376−384. (c) Han, Z.; McNamara, W. R.; Eum, M.-S.; Holland, P. L.; Eisenberg, R. A Nickel Thiolate Catalyst for the Long-Lived Photocatalytic Production of Hydrogen in a Noble-Metal-Free System. *Angew. Chem., Int. Ed.* **2012**, *51*, 1667−1670. (d) Orain, C.; Quentel, F.; Gloaguen, F. Photocatalytic Hydrogen Production Using Models of the Iron−Iron Hydrogenase Active Site Dispersed in Micellar Solution. *ChemSusChem* **2014**, *7*, 638−643. (e) Li, X.; Wang, M.; Zheng, D.; Han, K.; Dong, J.; Sun, L. Photocatalytic H_2

https://doi.org/10.1021/acscatal.3c01347
ACS Catal. 2023, 13, 9476−9486

production in aqueous solution with host-guest inclusions formed by insertion of an FeFe-hydrogenase mimic and an organic dye into cyclodextrins. *Energy Environ. Sci.* **2012**, *5*, 8220−8224. (f) McCormick, T. M.; Han, Z.; Weinberg, D. J.; Brennessel, W. W.; Holland, P. L.; Eisenberg, R. Impact of Ligand Exchange in Hydrogen Production from Cobaloxime-Containing Photocatalytic Systems. *Inorg. Chem.* **2011**, *50*, 10660−10666. (g) Sabatini, R. P.; Eckenhoff, W. T.; Orchard, A.; Liwosz, K. R.; Detty, M. R.; Watson, D. F.; McCamant, D. W.; Eisenberg, R. From Seconds to Femtoseconds: Solar Hydrogen Production and Transient Absorption of Chalcogenorhodamine Dyes. *J. Am. Chem. Soc.* **2014**, *136*, 7740−7750. (h) Zhang, P.; Wang, M.; Dong, J.; Li, X.; Wang, F.; Wu, L.; Sun, L. Photocatalytic Hydrogen Production from Water by Noble-Metal-Free Molecular Catalyst Systems Containing Rose Bengal and the Cobaloximes of BFx-Bridged Oxime Ligands. *J. Phys. Chem. C* **2010**, *114*, 15868−15874.

(25) (a) Puckett, C. A.; Barton, J. K. Mechanism of cellular uptake of a ruthenium polypyridyl complex. *Biochemistry* **2008**, *47*, 11711−11716. From NLM (b) Liu, P.; Liu, J.; Zhang, Y.-Q.; Wu, B.-Y.; Wang, K.-Z. Synthesis, DNA binding and photocleavage, and cellular uptake of an alkyl chain-linked dinuclear ruthenium(II) complex. *J. Photochem. Photobiol., B* **2015**, *143*, 89−99.

(26) Lai, M.; Lü, B. Tissue Preparation for Microscopy and Histology. In *Comprehensive Sampling and Sample Preparation*; Pawliszyn, J., Ed.; Academic Press, 2012; pp 53−93.

(27) (a) Okura, I.; Kobayashi, M.; Kim-Thuan, N.; Nakamura, S.; Nakamura, K.-I. Photoreduction of methyl viologen by triphenylamine and hydrogen generation with hydrogenase. *J. Mol. Catal.* **1980**, *8*, 385−390. (b) Hoogvliet, J. C.; Lievense, L. C.; van Dijk, C.; Veeger, C. Electron transfer between the hydrogenase from Desulfovibrio vulgaris (Hildenborough) and viologens. 2. Investigations by chronoamperometry. *Eur. J. Biochem.* **1988**, *174*, 281−285.

(28) Sanchez, M. L. K.; Wu, C.-H.; Adams, M. W. W.; Dyer, R. B. Optimizing electron transfer from CdSe QDs to hydrogenase for photocatalytic H_2 production. *Chem. Commun.* **2019**, *55*, 5579−5582.

(29) Michaelis, L.; Hill, E. S. The Viologen Indicators. *J. Gen. Physiol.* **1933**, *16*, 859−873.

(30) Adamska-Venkatesh, A.; Krawietz, D.; Siebel, J.; Weber, K.; Happe, T.; Reijerse, E.; Lubitz, W. New Redox States Observed in [FeFe] Hydrogenases Reveal Redox Coupling Within the H-Cluster. *J. Am. Chem. Soc.* **2014**, *136*, 11339−11346.

(31) Jones, R. W.; Garland, P. B. Sites and specificity of the reaction of bipyridylium compounds with anaerobic respiratory enzymes of Escherichia coli. Effects of permeability barriers imposed by the cytoplasmic membrane. *Biochem. J.* **1977**, *164*, 199−211.

(32) (a) Rosenbaum, M.; Aulenta, F.; Villano, M.; Angenent, L. T. Cathodes as electron donors for microbial metabolism: Which extracellular electron transfer mechanisms are involved? *Bioresour. Technol.* **2011**, *102*, 324−333. (b) Rabaey, K.; Rozendal, R. A. Microbial electrosynthesis—revisiting the electrical route for microbial production. *Nat. Rev. Microbiol.* **2010**, *8*, 706−716.

(33) (a) Amouyal, E.; Keller, P.; Moradpour, A. Light-induced hydrogen generation from water catalysed by ruthenium dioxide. *J. Chem. Soc., Chem. Commun.* **1980**, *21*, 1019−1020. (b) Kaeffer, N.; Morozan, A.; Fize, J.; Martinez, E.; Guetaz, L.; Artero, V. The Dark Side of Molecular Catalysis: Diimine−Dioxime Cobalt Complexes Are Not the Actual Hydrogen Evolution Electrocatalyst in Acidic Aqueous Solutions. *ACS Catal.* **2016**, *6*, 3727−3737.

(34) Gohn, M.; Getoff, N. Homogeneous Photoredox System for Hydrogen Production by Solar-Energy. *Z Naturforsch A* **1979**, *34*, 1135−1139.

(35) Pellegrin, Y.; Odobel, F. Sacrificial electron donor reagents for solar fuel production. *C. R. Chim.* **2017**, *20*, 283−295.

(36) (a) Sakai, K.; Kizaki, Y.; Tsubomura, T.; Matsumoto, K. Homogeneous catalyses of mixed-valent octanuclear platinum complexes in photochemical hydrogen production from water. *J. Mol. Catal.* **1993**, *79*, 141−152. (b) Keller, P.; Moradpour, A. Is there a particle-size dependence for the mediation by colloidal redox catalysts of the light-induced hydrogen evolution from water? *J. Am. Chem. Soc.* **1980**, *102*, 7193−7196.

(37) Venturi, M.; Mulazzani, Q. G.; Hoffman, M. Z. Radiolytically-induced one-electron reduction of methyl viologen in aqueous solution: Stability of the radical cation in acidic and highly alkaline media(1). *Radiat. Phys. Chem.* **1984**, *23*, 229−236.

(38) Tanaka, S.; Masaoka, S.; Yamauchi, K.; Annaka, M.; Sakai, K. Photochemical and thermal hydrogen production from water catalyzed by carboxylate-bridged dirhodium(ii) complexes. *Dalton Trans.* **2010**, *39*, 11218−11226.

(39) (a) Kuchenreuther, J. M.; Grady-Smith, C. S.; Bingham, A. S.; George, S. J.; Cramer, S. P.; Swartz, J. R. High-Yield Expression of Heterologous [FeFe] Hydrogenases in Escherichia coli. *PLoS One* **2010**, *5*, No. e15491. (b) Siebel, J. F.; Adamska-Venkatesh, A.; Weber, K.; Rumpel, S.; Reijerse, E.; Lubitz, W. Hybrid [FeFe]-Hydrogenases with Modified Active Sites Show Remarkable Residual Enzymatic Activity. *Biochemistry* **2015**, *54*, 1474−1483.

(40) Kitzler, J.; Fridovich, I. The effects of paraquat on Escherichia coli: Distinction between bacteriostasis and lethality. *Free Radical Biol. Med.* **1986**, *2*, 245−248.

(41) Bus, J. S.; Gibson, J. E. Paraquat: model for oxidant-initiated toxicity. *Environ. Health Perspect.* **1984**, *55*, 37−46.

(42) Macii, F.; Detti, R.; Bloise, F. R.; Giannarelli, S.; Biver, T. Spectroscopic Analysis of the Binding of Paraquat and Diquat Herbicides to Biosubstrates. *Int. J. Environ. Res. Public Health* **2021**, *18*, 2412.

(43) Gray, J. P.; Heck, D. E.; Mishin, V.; Smith, P. J. S.; Hong, J.-Y.; Thiruchelvam, M.; Cory-Slechta, D. A.; Laskin, D. L.; Laskin, J. D. Paraquat Increases Cyanide-insensitive Respiration in Murine Lung Epithelial Cells by Activating an NAD(P)H:Paraquat Oxidoreductase: Identification Of The Enzyme As Thioredoxin Reductase. *J. Biol. Chem.* **2007**, *282*, 7939−7949.

(44) (a) Hiraishi, T.; Kamachi, T.; Okura, I. Kinetic studies of electron transfer on photoinduced hydrogen evolution with hydrogenase. *J. Photochem. Photobiol., A* **1996**, *101*, 45−47. (b) Pavliuk, M. V.; Lorenzi, M.; Morado, D. R.; Gedda, L.; Wrede, S.; Mejias, S. H.; Liu, A.; Senger, M.; Glover, S.; Edwards, K.; et al. Polymer Dots as Photoactive Membrane Vesicles for [FeFe]-Hydrogenase Self-Assembly and Solar-Driven Hydrogen Evolution. *J. Am. Chem. Soc.* **2022**, *144*, 13600−13611.

(45) Watanabe, T.; Honda, K. Measurement of the extinction coefficient of the methyl viologen cation radical and the efficiency of its formation by semiconductor photocatalysis. *J. Phys. Chem.* **1982**, *86*, 2617−2619.

(46) Tazuke, S.; Kitamura, N.; Kawanishi, Y. Problems of back electron transfer in electron transfer sensitization. *J. Photochem.* **1985**, *29*, 123−138.

https://doi.org/10.1021/acscatal.3c01347
ACS Catal. 2023, 13, 9476−9486